Braz J Phys (2016) 46:547–555
DOI 10.1007/s13538-016-0434-3

STATISTICAL

Thermal Lens Phenomenon Studied by the Z-Scan Technique: Measurement of the Thermal Conductivity of Highly Absorbing Colloidal Solutions

A. L. Sehnem[1] · D. Espinosa[1] · E. S. Gonçalves[1] · A. M. Figueiredo Neto[1]

Received: 24 May 2016 / Published online: 20 July 2016

Abstract We discuss the thermal lens phenomenon in high-absorbing colloidal systems, studied by using the Z-scan technique. The characteristics of the experimental setup to avoid undesirable effects are presented, in particular when pulsed laser beam is used. We show that a cumulative effect may appear in the experiment with chopped laser beams and compromise the results obtained with this technique. This artefact is more significative when colloidal suspensions are investigated. These materials have different characteristic times of heat and mass diffusion, which must be carefully considered to choose the appropriate time interval for the laser pulse and the time between pulses. Two experimental cases with a chopped laser beam, with and without a shutter, are discussed. The sample employed is a magnetic colloidal suspension (a ferrofluid). This sample has magnetic nanoparticles electrically charged in an aqueous solution with free ions and counter ions. Besides the thermal lens effect, charge and mass diffusion may take place when the sample is illuminated by the Gaussian beam, which imposes a thermal gradient on it. The results show that, with the experimental setup without a shutter, the sample does not achieve a complete relaxation between two laser pulses. This generates a measurable cumulative effect after the sample is illuminated during a relatively long period of time. A time modulation with longer time interval between chopped pulses allows the complete relaxation of the sample. This procedure is important for the correct analysis of the thermal lens effect. Reliable values of the thermal conductivity of the sample in different temperatures are obtained and discussed.

Keywords Thermal lens · Z-scan technique · Colloidal systems · Accumulated thermal effects · Thermal conductivity

1 Introduction

Thermal lens optical phenomenon is widely used to investigate thermal and optical properties of materials, like thermal conductivity and diffusivity and low absorption coefficients in complex fluids [1–7]. The thermo-optical properties of various materials such as liquid crystals, colloidal solutions [8–12] and liquid mixtures [13] can be investigated inducing the formation of a thermal lens on them. It is also possible to apply this method to biological solutions of HDL and LDL (high and low-density lipoproteins) [14] and plasma from human blood [15].

The single-beam Z-scan experimental technique [16] is widely used to investigate the thermal lens effect on materials [17–19]. This technique is based on the sample self-focusing (defocusing) effect on a previously focused Gaussian laser beam [20–22]. Light absorbed by the sample is converted into heat that spreads to non-illuminated regions of the sample. This process induces a refraction index gradient across the sample, generating the thermal lens effect. This refraction index gradient is related to the thermo-optic coefficient dn/dT (n is the refraction index and T is the absolute temperature) that depends on the sample properties. The rate and amplitude of thermal lens sample response

✉ A. L. Sehnem
alsehnem@if.usp.br

[1] Instituto de Física, Universidade de São Paulo, São Paulo, Brazil

depend on the thermal diffusivity and thermal conductivity of the material.

The thermal lens characteristic signal from a sample in the Z-scan experiment shows a peak-to-valley (or valley-to-peak) behaviour, represented by the z-dependence of the light beam transmittance [18]. In this case, the light transmitted by the sample is collected by a detector (in the far field) with an iris in front of it, as a function of time for each z position of the sample. If the induced thermal lens is of the divergent type, i.e. $dn/dT < 0$, the light transmittance increases as a function of time for $z < 0$ and decreases for $z > 0$ ($z = 0$ is the beam focus position). Usually in the Z-scan technique (in the case of the study of thermal effects), the light beam is pulsed by using a mechanical chopper. It provides a sequence of square pulses in the time scale of milliseconds, creating a periodic light incident beam on the sample. The time interval Δt that the sample is illuminated by the beam is equal to the time interval the laser beam is interrupted by the chopper blade. The choice of this time interval is critical to obtain reliable data. If this time interval is too short, compared to the typical thermal characteristic time t_{th}, the thermal lens does not reach the stationary state and, in the next laser pulse, the system did not relax back completely, and a cumulative effect is present during the measurement [23, 24]. On the other hand, if $\Delta t \gg t_{th}$, other effects can be triggered in the sample, e.g. the Soret effect (or thermodiffusion) [25], introducing artefacts in the experimental data. These experimental artefacts appear, and can be identified, in the transmittance recorded by the detector just when the chopper opens and illuminates the sample. We will call this measurement of the transmittance at $t = 0$ in a given laser pulse "the first experimental point—FEP" recorded at a z position of the sample, when the laser pulse illuminates the sample. It is important to stress that, in a typical time-resolved thermal lens experiment, this FEP should be independent of the z position of the sample. In colloidal systems, where the light absorbers have mobility in the fluid carrier, it is essential to get rid of all additional thermal processes to investigate just thermal lens properties of the sample.

In this work, we focus on an unexpected behaviour that can be observed in the Z-scan experiment in colloidal systems, analysing the FEP of the laser pulse transmitted by the sample. We will show that in the investigation of the thermal lens phenomenon in colloidal solutions, it is possible to obtain a valley-to-peak (or peak-to-valley) behaviour from this FEP measured. The physical mechanism responsible for this behaviour is, sometimes, wrongly assumed to be from electronic origin. We will discuss the physical mechanism that is the source of this unexpected behaviour in the laser-chopped experiments. We will see that it is related to the cumulative effect of mass migration (thermal diffusion, also known as the Soret effect). This effect could happen during the formation of the thermal lens itself, if the chopped beam has $\Delta t \sim t_{th}$ [23]. A step-by-step analysis will be described to correctly obtain the (previously unknown) thermal conductivity of a colloidal sample in the thermal lens Z-scan experiment. As a working example, we performed the Z-scan thermal lens experiment with an aqueous ionic ferrofluid [26], as a function of temperature of the solution.

2 Thermal Lens: Theory and Experiment

The thermal lens effect is induced by a focused Gaussian beam incident on a sample, due to light absorption, generating a radial temperature gradient on it [27–30]. The temperature profile is calculated by solving the radial heat transport equation [31]. A radial refractive index gradient is established in the sample due to the local thermal expansion of the material, producing the lens effect. Figure 1 illustrates the beam defocusing effect generated by the sample heating. In this example, the beam waist increases in the far-field position, where a detector with an iris in its front registers the on-axis transmittance. Gordon et al. [27] described the focal length of the thermal lens generated in a sample illuminated by a non-focused Gaussian beam. Whinnery and Hu extended this calculation to the case of a focused Gaussian beam [20, 21]. These two calculations use a parabolic approximation to the refractive index profile. A different model was developed by Sheldon et al. [28] considering the aberrant nature of the lens. Both models were reviewed by Carter and Harris [32] to obtain the thermal lens amplitude and thermal diffusivity of weakly absorbing materials. In the present work, we will use the parabolic approximation, briefly described below.

2.1 Parabolic Model

Assuming the Gaussian beam light absorption in a cylindrical section of the sample that acts as a source of heat, the temperature increase is given by

$$\Delta T\,(r,t) = \frac{0.06\alpha P}{\pi\kappa}\left[Ei\left(-\frac{2r^2}{w^2}\right) - Ei\left(-\frac{2r^2}{8D_{th}t + w^2}\right)\right], \tag{1}$$

where α is the light absorption coefficient, P is the irradiating beam power, κ is the thermal conductivity of the sample and $Ei(x)$ is the exponential integral function. The variable r is the radial distance with respect to the centre of the beam, and w is the beam radius (waist) at the sample. The thermal diffusivity is defined as $D_{th} = \kappa/\rho C_p$, where ρ and C_p are the mass density and specific heat capacity of the sample. As the iris aperture (Fig. 1) is much smaller than the beam

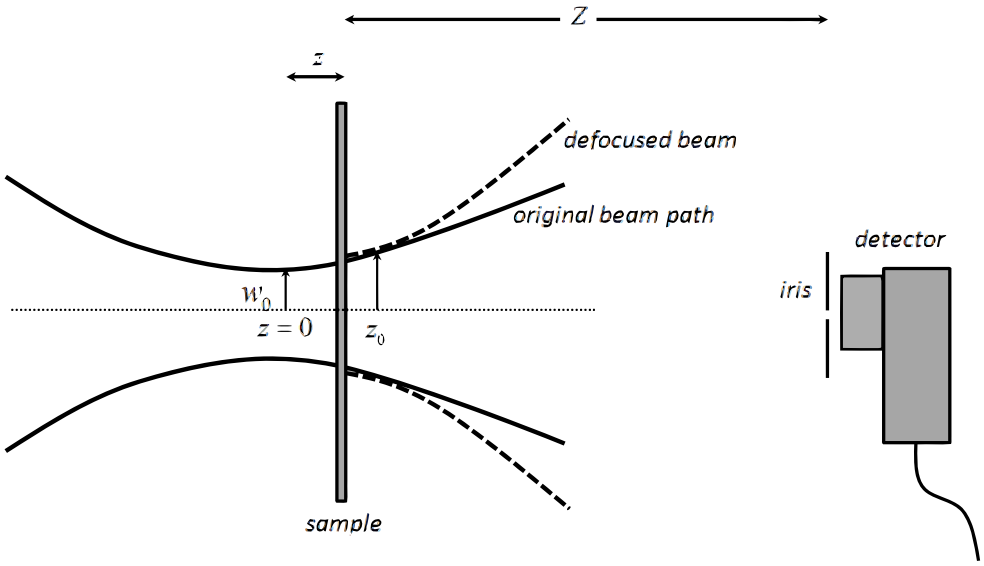

Fig. 1 Schematic view of the thermal lens defocusing effect: the *solid line* corresponds to the original beam path and the *dashed line* to the path after sample is heated by the focused Gaussian beam

waist at the sample position z, a parabolic approximation to (1) leads to

$$\Delta T\,(r,t) = \frac{0.06\alpha P}{\pi\kappa}\left[ln\left(1+\frac{2t}{t_{th}}\right) - \frac{2r^2}{w^2}\left(\frac{2t}{2t+t_{th}}\right)\right], \tag{2}$$

with the characteristic time of heat diffusion $t_{th} = w^2/4D_{th}$. It is important to notice the number 0.06 that arises from the unit transformation of generated heat from (cal/cm.s) to the SI units, as indicated in [27, 28]. So special attention must be payed in the use of Eq. (2.2) and the unit system employed.

The refractive index of the sample is written as $n = n_0 + (dn/dT)\,\Delta T$. The focal length f of the thermal lens formed is [33]:

$$\frac{1}{f\,(t)} = -\,l_{eff}\frac{dn}{dT}\frac{d^2}{dr^2}\Delta T\,(r,t)\Big|_{r\to 0}, \tag{3}$$

where l_{eff} is the sample effective optical length. The normalised transmittance Γ_N is written as [34, 35]

$$\Gamma_N(z,t) = \frac{I(z,t)}{I(z,t=0)} = \left[1-2\gamma\frac{z_0}{f(t)} + \left(1+\gamma^2\right)\left(\frac{z_0}{f\,(t)}\right)\right]^{-1}, \tag{4}$$

where $\gamma = z/z_0$ is the relative sample position, $z_0 = \pi w_0^2/\lambda$ the Rayleigh length, λ the light wavelength and w_0 the beam waist at the focal position ($z = 0$). Γ_N may also be written as a function of the thermal lens amplitude $\theta = (0.24\,\alpha\ P\ l_{eff}/\kappa\ \lambda)\ dn/dT$:

$$\Gamma_N(z) = \frac{I(z,t)}{I(z,t=0)} = \left[1-2\gamma\left(\frac{\theta}{1+\gamma^2}\frac{2t}{2t+t_c}\right) + (1+\gamma^2)\left(\frac{\theta}{1+\gamma^2}\frac{2t}{2t+t_c}\right)^2\right]^{-1}. \tag{5}$$

To build up the Z-scan characteristic curve, we perform the following normalisation:

$$\Gamma_N(z) = \frac{\Gamma_N(z,0)}{\Gamma_N(z,t_\infty)}, \tag{6}$$

where t_∞ corresponds to the time that the thermal lens reached the stationary state.

This model predicts a maximum sample response at the positions $z = \pm\sqrt{2}z_0$. If it is possible to measure independently with good accuracy α, P, l_{eff} and dn/dT, the thermal lens Z-scan experiment can be used to obtain the thermal conductivity κ of the sample.

2.2 Experimental Thermal Lens Transient

Figure 2 presents a sketch of the experimental setup, where a chopper gives a sequence of square light pulses. The Gaussian beam of wavelength 532 nm is focused by the lens L1 on the chopper blade. The laser used is the cw Verdi, from Coherent Inc. A computer-controlled chariot moves the sample along the beam focus. After the sample, the beam is splitted for the analysis with two photodetectors: D1 analyses the beam refraction and D2 analyses the possible changes in the light absorption during the experiments. A shutter is also present in the setup, and the convenience of its use in an experiment will be discussed in the following. Considering a focused Gaussian beam with typical waist $w_0 \sim 30\mu m$ and a sample of thermal diffusivity $D_{th} \sim 10^{-7}$ m^2/s, the heat diffusion time is a few milliseconds. The sample investigated in our experiment is an ionic magnetic colloidal suspension (also named ferrofluid), constituted of $CoFe_2O_4$ magnetic nanoparticles, average diameter 13.6 nm, dispersed in aqueous nitric-acid solution 0.1 M [36, 37]. This ferrofluid was recently employed in an investigation to measure its Soret coefficient [25]. For this

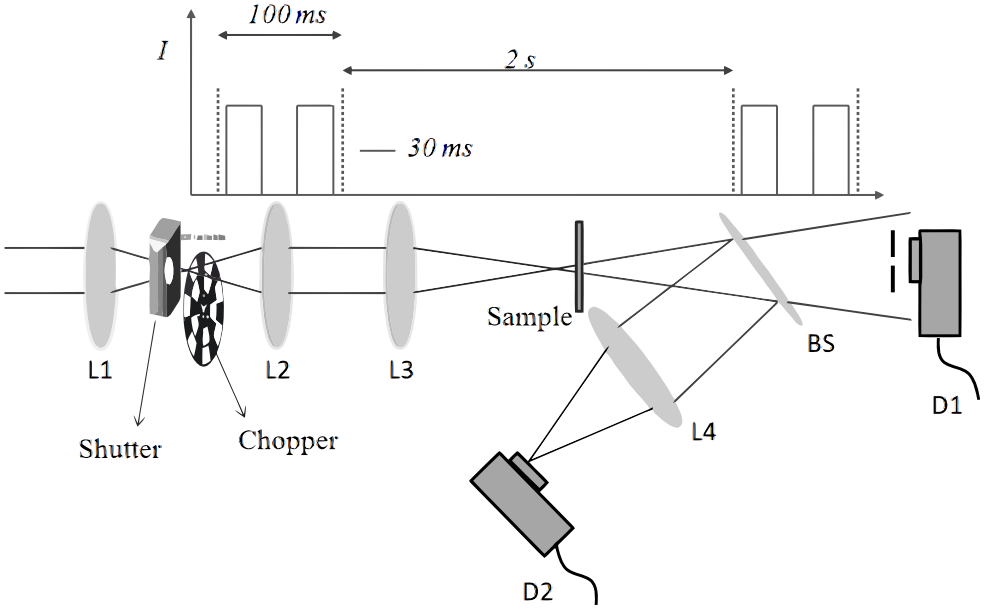

Fig. 2 Schematic view of the experimental setup for the thermal lens experiment, showing the propagation of the Gaussian beam trough the optical elements. The upper schema shows the light modulation by using the shutter and the chopper

type of material, light pulse of $\Delta t = 30$ ms is enough to detect the transient of the thermal lens effect, measuring the time evolution of the transmitted intensity.

We will perform the analysis of the thermal lens transient in two cases: the first one (I), when only the chopper is used to create the 30-ms periodic modulation of the laser beam; in the second case (II), a shutter is placed before the chopper and blocks the beam during 2 s between a sequence of two square pulses (see Fig. 2).

Case (I) Figure 3a shows the time evolution of the light transmittance (raw data obtained in the photodetector) with the sample in two different z positions, before and after the beam focus position (sample at $z \sim \pm\sqrt{2}z_0$). The data represent the absolute values of the transmitted intensity of the square pulses, representing an average of 10 independent measurements at each z position. The different values of the transmittance (in the FEP) in both curves are clearly observed. If only the thermal lens effect occurred, the curves should start at the same transmittance value. The plot of the transmittance of the FEP (normalised by the transmittance value obtained with the sample in a z position far from the beam focus), as a function of z, is presented in Fig. 3b, showing an unexpected valley-to-peak behaviour. The results in Fig. 3b can lead to a wrong interpretation that the normalised transmittance of the FEP changes with z due to electronic optical mechanisms that occur at time scales faster than milliseconds, as the optical Kerr effect [38]. A detailed description of the physical mechanism that generates this behaviour will be given in the following.

Case (II) The same experiment was performed now with the chopper and the shutter present. We choose 30-ms square periodic pulses created by the chopper and modulate themselves by a 100-ms opened window and 2-s closed window with a shutter, as shown in the upper sketch in Fig. 2. The time evolution of the light transmittance (raw data, sample at $z \sim \pm\sqrt{2}z_0$) is shown in Fig. 4a. In this case, different from the results shown in Fig. 3a, the initial values of the transmittance (FEP) in both curves are the same. This occurs for all the z positions of the sample and is shown in Fig. 4b (the same normalisation procedure described in case (I) was employed here). The results shown in Fig. 4b clearly indicate that the behaviour of the FEP in the Z-scan experiment shown in Fig. 3b is not due to mechanisms faster than milliseconds. Otherwise, the results of Figs. 4b and 3b would be the same. In other words, none of the results with shutter + chopper combination resulted in any lens effect of the FEP from electronic origin. Electronic effects, like the two-photon absorption, have a faster characteristic time, of the order of femtoseconds. This effect may be investigated by using a pulsed fs laser, which is not the aim of the present work.

The behaviour observed in Fig. 3b (experimental case I) can be explained considering the mass diffusion effect generated by the temperature gradient established in the illuminated region of the sample, due to the chopped laser pulse. While the chopped light pulses of $\Delta t = 30$ ms heat the sample, the nanoparticles dispersed in water respond to the temperature gradient corresponding to the Soret effect. In the present case of ferrofluids with positively charged particles, the faster response comes from the free nitrate and hydronium ions present in the sample subjected to a temperature gradient. The characteristic response time of the charged nanoparticles and the ions to the thermal gradient, associated with the mass thermodiffusion phenomenon,

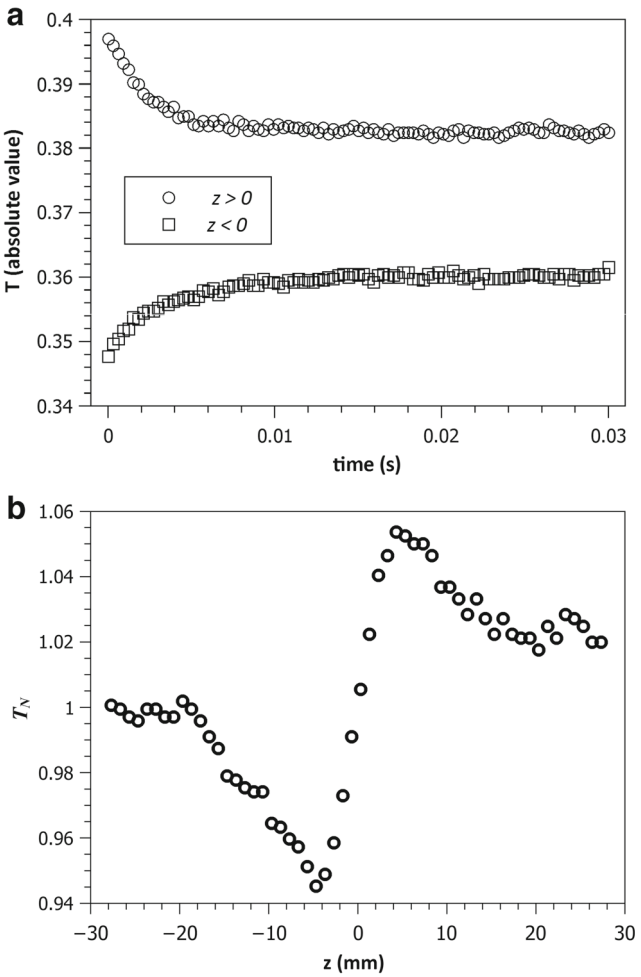

Fig. 3 Experimental case I, where the laser beam is chopped. **a** Time evolution of the transmittance of the sample in two z positions. The transmittance is expressed in absolute values given by the photodetector. **b** Normalised transmittance of the first experimental point (FEP at $t = 0) T_N = I(z, t = 0)/I(z \to \infty, t = 0)$ as a function of z. $z \to \infty$ means a z position far from the focus, where the thermal lens effect is assumed to be absent

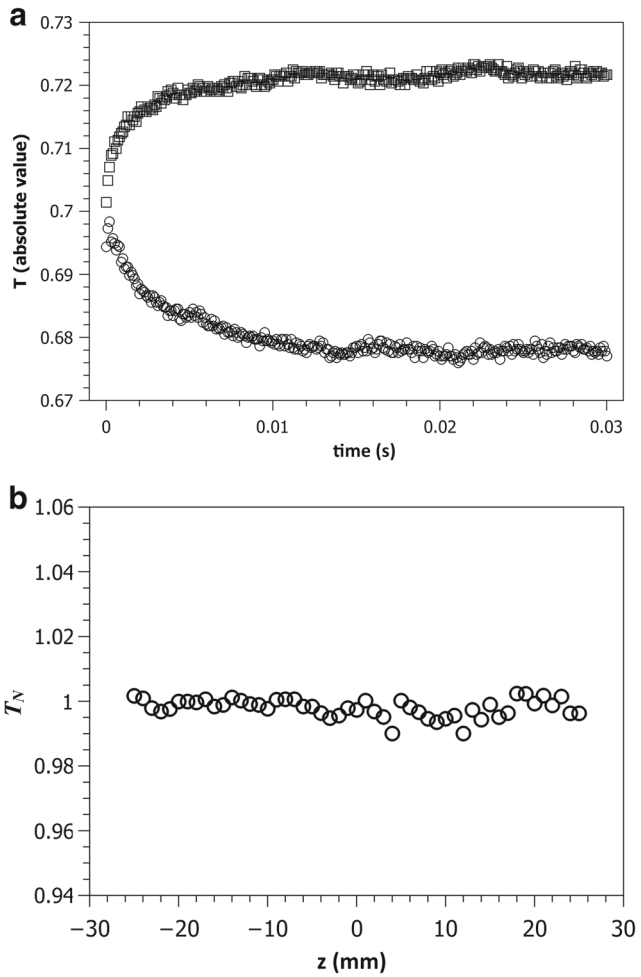

Fig. 4 Experimental case II, where the laser beam is modulated by using the shutter and the chopper. **a** Time evolution of the transmittance of the sample in two z positions. The transmittance is expressed in absolute values given by the photodetector. **b** Normalised transmittance of the first experimental point (FEP, at $t = 0) T_N = I(z, t = 0)/I(z \to \infty, t = 0)$ as a function of z. $z \to \infty$ means a z position far from the focus, where the thermal lens effect is assumed to be absent

is different. The mass diffusion time is given by $t_c = w^2/4D_M$, with D_M being the mass diffusion coefficient of the ions or nanoparticles [39, 40]. It is of the order of hundreds of milliseconds for ions and tens of seconds for nanoparticles. The movement of the nanoparticles is, in part, caused by the thermoelectric field created by the ionic Soret effect [25, 41]. The irradiating time of 30 ms is enough to generate a small ionic concentration gradient in the sample. In the next 30 ms, when the laser is turned off, there is not a complete relaxation of the ionic gradient established and it continues to increase in the next irradiating pulse, and so on. Figure 5 illustrates the way that the thermoelectric field evolves in the chopped-beam experiment. An analogous behaviour was reported by Fang and Swofford [24], where a cumulative effect on the thermal lens itself is described. In the case of our sample, the thermoelectric field created acts during all the time the experimental results shown in Fig. 3 were taken. It induces the nanoparticle concentration gradient, which is the matter lens observed in Fig. 3b. This thermoelectric field increases as the sample approaches the beam focus, due to the higher light intensity. In a typical Z-scan experiment, 10 independent measurements of the thermal lens transient are recorded at each z position, with 1 s of interval between each acquisition. After that, an average time evolution curve (those shown in Fig. 3a) is obtained. Under these experimental conditions, the sample remains about 15 s in each z position during which approximately 250 cycles of turning on and off the light beam occur. In this total time, noticeable particle and ion concentration gradients are established. This phenomenon is responsible for the behaviour of the FEP measured in the time evolution of the transmittance curve.

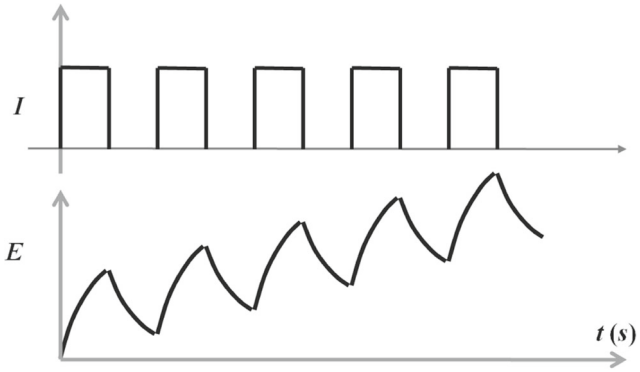

Fig. 5 Sketch of the chopped light beam intensity I and the cumulative thermoelectric field E established in the ionic ferrofluid sample due to the ionic Soret effect

When the shutter is employed in the setup, as indicated in Fig. 2, only two chopped pulses reach the sample during the time the shutter is opened. During the following 2 s, when the shutter is closed, the sample has time to completely relax the low ionic concentration gradient induced. In this case, the matter lens is not formed, as shown in Fig. 4. This is an important result since the undesired effect of mass diffusion can introduce artefacts in the study of the thermal lens effect on colloidal solutions. Figure 6 shows the normalised transmittance $\Gamma_N(z)$ experimentally obtained for both cases I and II. An important and unexpected asymmetry of the Z-scan characteristic curve and a bigger peak-to-valley amplitude is observed in the results obtained according to the case I procedure. The curve obtained in case II shows a more symmetric aspect and a smaller peak-to-valley amplitude.

The accumulated matter lens effect described above can be present in previously reported experiments performed with pulsed laser light in colloidal systems [42, 43]. The beams used were light pulses separated by millisecond or even microsecond time intervals, enabling the formation of the thermal lens, but also the cumulative formation of the matter lens. This effect has been considered as an "accumulated thermal effect" and was observed also in dye [44] and polymer [45] solutions. In conclusion, the peak-to-valley behaviour of the Z-scan results may contain contributions from thermal and matter lens, besides the electronic self-focusing effect. Much attention must be paid in the identification of each one of these contributions in the measurement to the correct interpretation of the experimental results.

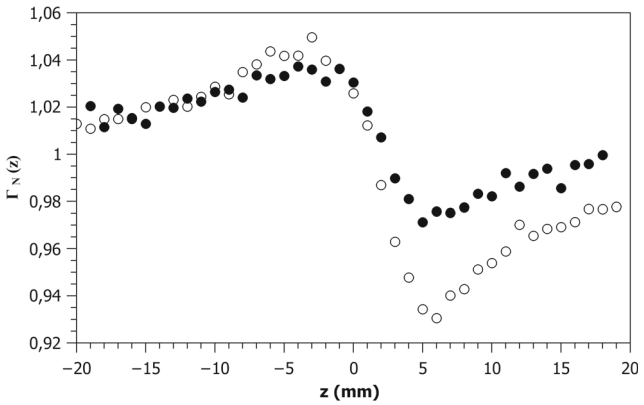

Fig. 6 Z-Scan typical curve in the time scale of the thermal lens phenomenon. Normalised transmittance $\Gamma_N(z)$ as a function of z: case I (*white circle*), case II (*black circle*)

3 Analysis of the Thermal Lens Results

Now, we are able to obtain the thermal lens experimental results, employing the Z-scan apparatus, without the influence of the Soret phenomenon. The experiment presented below is a working example performed according to case II. We will investigate the temperature dependence of the sample thermal conductivity measured by using the Z-scan technique, in the framework of the parabolic thermal lens model. All the other characteristic parameters of the sample present in the expression of the lens amplitude θ were measured independently, or obtained from the literature.

The volume fraction of nanoparticles in the solution was very low ($\phi \sim 0.075$ %) and the solution absorption coefficient was $\alpha = (29 \pm 2)$ cm^{-1} at 532 nm. It is a relatively high absorption coefficient but we neglected the possible effect of axial heat propagation as the sample effective length changes only around 10 % relative to sample thickness $l = 80$ μm and $l_{eff} \sim 72$ μm. The thermal lens experiments were performed inserting the sample in a hot stage temperature controller ($293K < T < 333K$), and the beam power used was 2.1 mW. The hot stage allows us to perform the thermal lens experiment as a function of the sample temperature.

The thermo-optic coefficient dn/dT was also precisely measured with an ATAGO 5000i refractometer with 2×10^{-5} nD accuracy. The temperature dependence of the

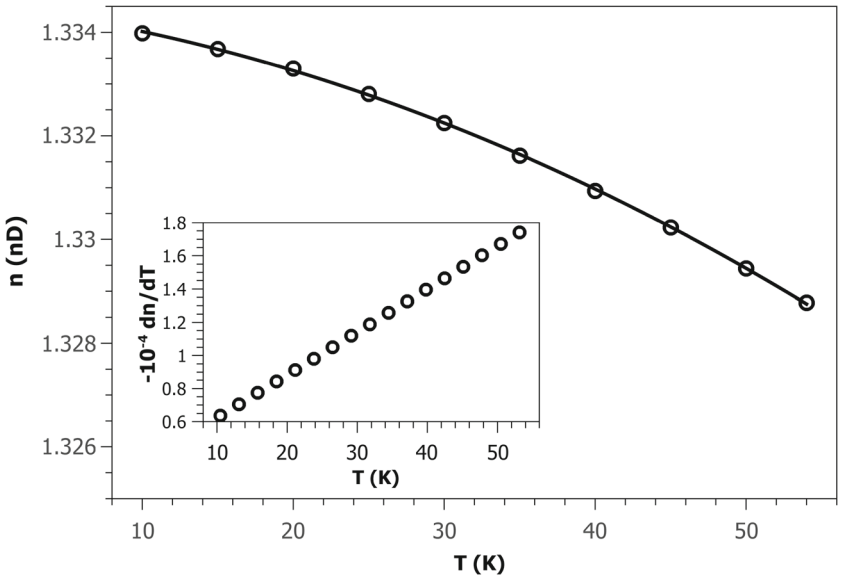

Fig. 7 Temperature dependence of the refractive index of the ferrofluid. The *inset* shows the temperature dependence of the thermo-optic coefficient dn/dT. *Solid line* represents a guide for eyes

refractive index of the ferrofluid is presented in Fig. 7. The insert shows $[dn/dT](T)$, where it is interesting to notice its linear temperature dependence, due to the parabolic dependence of the refractive index with T.

Figure 8 shows the experimental Z-scan curves ($\Gamma_N(z)$) and the fits with (6), where it is possible to see the influence of the temperature on the peak-to-valley amplitude of the curves. This behaviour comes from an interplay between the parameters dn/dT and κ. The unique fit parameter is the thermal conductivity of the sample. The obtained temperature dependence of the thermal conductivity is shown in Fig. 9 and compared with the values of pure water [46].

As expected, the thermal conductivity of our water-base ferrofluid is essentially that of water, except at $T > 50\,°C$, where the values show a tendency to be larger than those from pure water. The ferrofluid contains magnetic nanoparticles immersed in 10 mM HNO_3 solution, and these solutes are expected to increase the heat conduction. The free ion contribution to the heat conduction is expected to be smaller than 3 % [3]. Lee et al. [47] have shown that the influence of the (semiconductor) nanoparticles depends on the surface charge complexation, resulting in a higher thermal conductivity for nanoparticle solution, with higher zeta potential. In a previous work [25], the increasing of the zeta potential with temperature was shown, and this can be reflected in

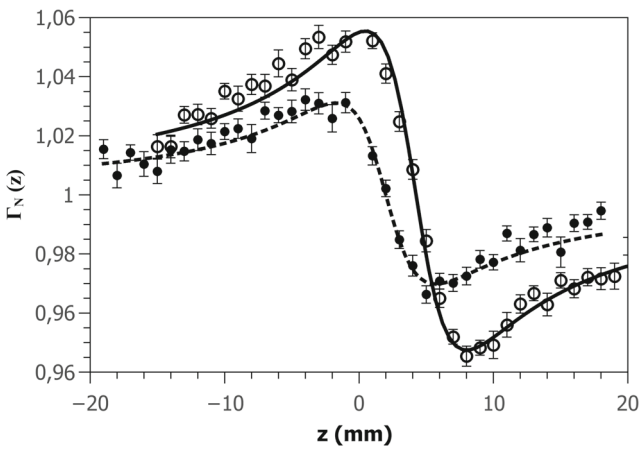

Fig. 8 Z-Scan typical curve in the time-scale of the thermal-lens phenomenon. Normalised transmittance $\Gamma_N(z)$ as a function of z, case II: $T = 293K(\bullet)$; $T = 343K(\circ)$. Continuous and dashed lines are fits with (6)

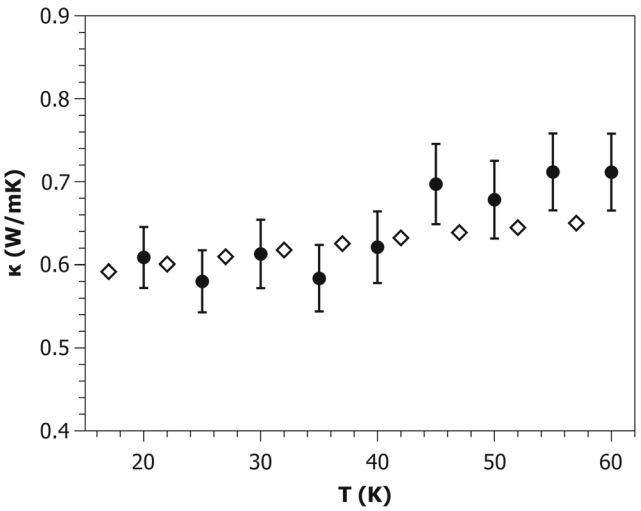

Fig. 9 Temperature dependence of the thermal conductivity obtained for the ferrofluid sample (*black circle*) compared with that of pure water (*white diamond*)

the higher thermal conductivity of the ferrofluid for higher temperatures. In the present work, the contribution from the nanoparticles to the thermal conductivity measured is expected to be low, due to the small volume fraction of them in our samples. For example, the classical Maxwell's model [48] predicts a thermal conductivity enhancement lower than 5 % due to the presence of 0.075 vol% cobalt ferrite nanoparticles in water (assuming $\kappa < 100$ $\mathrm{Wm^{-1}\,K^{-1}}$ for cobalt-ferrite nanoparticles). Even the newest and more refined models predict values below this limit [49].

If we use the Z-scan results obtained according to the procedure described in case I (open circles in Fig. 6), the thermal conductivity obtained by fitting expression (6) to the data is about (0.4 ± 0.1) $\mathrm{Wm^{-1}\,K^{-1}}$ that certainly is not expected for a diluted water-base ferrofluid.

4 Conclusions and Perspectives

In this work, we show that, depending on the experimental conditions, the thermal lens Z-scan experiment may bring cumulative thermal effects (e.g. thermodiffusion) that can introduce artefacts that compromise the analysis of the thermal lens experiment. This is particularly critical when chopped laser beams are used in the apparatus. This effect can be avoided by placing a shutter before the chopper and adjusting the time interval between pulses to allow the sample to relax back to the initial state (before the incidence of the beam). As a working example, we measured the thermal conductivity of a ferrofluid and show how additional phenomena, besides the thermal lens, may contaminate the experimental data and, as a consequence, the final results. As a final remark, the parabolic lens model used in the present investigation works well, despite the model limitations. A comparison with newer lens models (e.g. based on the aberrant lens model) can be the subject of forthcoming studies, being beyond the scope of the present investigation. Here, we emphasise the importance of the experimental procedure (independent on the thermal lens model) to obtain reliable results.

References

1. M.L. Baesso, J.R.D. Pereira, A.C. Bento, A.J. Palangana. Braz. J. Phys., 28 (1998)
2. J.H. Rohling, J. Mura, J.R.D. Pereira, A.J. Palangana, A.N. Medina, A.C. Bento, M.L. Baesso. Braz. J. Phys. **32**, 575 (2002)
3. J. Georges. Spect. Acta Part A **69**, 1063 (2008)
4. N.G.C. Astrath, F.B.G. Astrath, J. Shen, J. Zhou, P.R.B. Pedreira, L.C. Malacarne, A.C. Bento, M.L. Baesso. Opt. Lett. **33**, 1464 (2008)
5. C.V. Bindhu, S.S. Harilal, V.P.N. Nampoori, C.P.G. Vallabhan. Opt. Eng. **37**, 2791 (1998)
6. N.G.C. Astrath, J. Shen, M.L. Baesso, F.B.G. Astrath, L.C. Malacarne, P.R.B. Pedreira, A.C. Bento, J. Zhou. J. Phys. Conf. Ser. **214**, 012014 (2010)
7. M. Benitez, A. Marcano, N. Melikechi. Opt. Eng. **48**, 043604 (2009)
8. P.B. de Melo, A.M. Nunes, L. Omena, S.M.S. do Nascimento, M.G.A. da Silva, M.R. Meneghetti, I.N. de Oliveira. Phys. Rev. E **92**, 042504 (2015)
9. V.M. Lenart, R.F. Turchiello, G.F. Goya, S.L. Gómez. Braz. J. Phys. **45**, 213 (2015)
10. R. Gutiérrez Fuentes, J.F. Sánchez Ramírez, J.L. Jiménez Pérez, J.A. Pescador Rojas, E. Ramón-Gallegos, A. Cruz-Orea. Int. J. Thermophys. **28**, 1048 (2007)
11. S.L. Gómez, V.M. Lenart, R.F. Turchiello, I.H. Bechtold, A.A. Vieira, H. Gallardo. Liq. Cryst. **43**, 268 (2015)
12. J.R.D. Pereira, A.M. Mansanares, A.J. Palangana, M.L. Baesso. Phys. Rev. E **64**, 012701 (2001)
13. N. Arnaud, J. Georges. Spectrochim. Acta, Part A **60**, 1817 (2004)
14. A.M. Monteiro, M.A.N. Jardini, V. Giampaoli, S. Alves, A.M. Figueiredo Neto, M. Gidlund. J. Biomedical Optics **17**, 115004 (2012)
15. J. Bernal-Alvarado, M. Sosa, R. Mayén-Mondragón, J.M. Yánez Limón, R. Flores-Farías, F. Hernández-Cabrera, P. Palomares. Instrum. Sci. Technol. **34**, 99 (2006)
16. M. Sheik-Bahae, A.A. Said, T.-H. Wei, D.J. Hagan, E.W. van Stryland. IEEE J. Quantum Electron **26**, 760 (1990)
17. F.L.S. Cuppo, A.M. Figueiredo Neto, S.L. Gómez, P. Palffy Muhoray. J. Opt. Soc. Am. B **19**, 1342 (2002)
18. F.L.S. Cuppo, A.M. Figueiredo Neto. Langmuir **18**, 9647 (2002)
19. C. Jacinto, D.N. Messias, A.A. Andrade, S.M. Lima, M.L. Baesso, T. Catunda. J. Non-Cryst. Solids **352**, 3582 (2006)
20. C. Hu, J.R. Whinnery. Applies Optics **12**, 72 (1973)
21. J.R. Whinnery. Acc. Chem. Res. **7**, 225 (1974)
22. N.J. Dovichi, J.M. Harris. Anal. Chem. **51**, 728 (1979)
23. H.L. Fang, R.L. Swofford, Vol. 3, *Ultrasensitive Laser Spectroscopy* (Academic Press, New York, 1983), p. 175ff
24. H.L. Fang, R.L. Swofford. J. Appl. Phys. **50**, 6609 (1979)
25. A.L. Sehnem, A.M. Figueiredo Neto, R. Aquino, A.F.C. Campos, F.A. Tourinho, J. Depeyrot. Phys. Rev. E **92**, 042311 (2015)
26. C. Sherer, A.M. Figueiredo Neto. Braz. J. Phys. **35**, 718 (2005)
27. J.P. Gordon, R.C.C. Leite, R.S. Moore, S.P.S. Porto, J.R. Whinnery. J. Appl. Phys. **36**, 3 (1965)
28. S.J. Sheldon, L.V. Knight, J.M. Thorne. Appl. Optics **21**, 1663–1669 (1982)
29. M. Sabeian, H. Rezaei. J. Eur. Opt. Soc.-Rapid **11**, 16004 (2016)
30. L.C. Malacarne, N.G.C. Astrath, M.L. Baesso. J. Opt. Soc. Am. B **29**, 1772 (2012)
31. H.S. Carslaw, J.C. Jaeger, *Conduction of Heat in Solids*, 2nd edn. (Oxford University Press, London, 1959)
32. C.A. Carter, J.M. Harris. Appl. Optics **23**, 476 (1984)
33. M. Born, E. Wolf, *Principles of Optics*, 4th edn. (Pergamon, Oxford, 1970), p. 124
34. A. Yariv, *Quantum Electronics*, 2nd edn. (Wiley, New York, 1975), p. 99ff
35. S.I.P.M.N. Alves, A. Bourdon, A.M. Figueiredo Neto. J. Opt. Soc. Am. B **20**, 713 (2003)
36. J.A. Gomes, M.H. Sousa, F.A. Tourinho, R. Aquino, G.J. da Silva, J. Depeyrot, E. Dubois, R. Perzynski. J. Phys. Chem. C **112**, 6220 (2008)
37. R. Aquino, F.A. Tourinho, R. Itri, M.C.F.L. Lara, J. Depeyrot. J. Magn. Magn. Mater. **252**, 23 (2002)
38. M. Sheik-Bahae, A.A. Said, E.W. Van Stryland. Opt. Lett. **14**, 955 (1989)
39. R. Rusconi, L. Isa, R. Piazza. J. Opt. Soc. Am. B **21**, 605 (2004)

40. N. Grofaniha, C. Conti, G. Ruocco, F. Zamponi. Phys. Rev. Lett., 038303 (2009)
41. A. Majee, A. Würger. Soft Matter **9**, 2145 (2013)
42. D. Soga, S. Alves, A. Campos, F.A. Tourinho, J. Depeyrot, A.M.F. Neto. J. Opt. Soc. Am. B **24**, 49 (2007)
43. C.P. Singh, K.S. Bindra, V. Shukla, J. Philip, A.K. Kar, J.E. McCarthy, H.T. Bookey. Adv. Sci. Eng. Med. **6**, 1 (2014)
44. K. Kamada, K. Matsunaga, A. Yoshino, K. Ohta. J. Opt. Soc. Am. B **20**, 529 (2003)
45. M. Falconieri, R.D. Amato, A. Furlani, M.V. Russo. Synth. Met. **124**, 217 (2001)
46. M.L.V. Ramires, C.A.N. Decastro, Y. Nagasaka, A. Nagashima, M.J. Assael, W.A. Wakeham. J. Phys. Chem. Ref. Data **24**, 1377 (1995)
47. D. Lee, J.W. Kim, B.G. Kim. J. Phys. Chem. B **110**, 4323 (2006)
48. J.C. Maxwell, *A Treatise on Electricity and Magnetism* (Oxford University Press, Cambridge, 1904)
49. E.K. Goharshadi, H. Ahmadzadeh, S. Samiee, M. Hadadian **1**, 1 (2013)